IEEE *Access*

Multidisciplinary : Rapid Review : Open Access Journal

Combination of Orthogonal Injections in Impedance Measurements of Grid-Connected Systems

HENRIK ALENIUS[1], (Student Member, IEEE), RONI LUHTALA[2], (Student Member, IEEE), and TOMI ROINILA[3], (Member, IEEE)
[1]Faculty of Information Technology and Communication Sciences, Tampere University, Finland (e-mail: henrik.alenius@tuni.fi)
[2]Faculty of Engineering and Natural Sciences, Tampere University, Finland (e-mail: roni.luhtala@tuni.fi)
[3]Faculty of Information Technology and Communication Sciences, Tampere University, Finland (e-mail: tomi.roinila@tuni.fi)

Corresponding author: Henrik Alenius (e-mail: henrik.alenius@tuni.fi).

ABSTRACT Impedance-based stability criterion has become a popular method in determining the stability of grid-connected systems. Recent studies have presented the utilization of various pseudo-random-sequence (PRS) perturbations for rapidly and accurately obtaining the impedances required for the stability analysis. A major drawback of the PRS is, however, that the signal power is linearly distributed over many harmonic frequencies. As the injection amplitude must be kept small to avoid too strong nonlinear distortions, it becomes challenging to provide enough power to the whole frequency band of interest.This work proposes a novel perturbation that is synthesized by summing up several independently designed orthogonal PRS injections. As the orthogonal sequences do not have power at common frequencies, the resulting combined signal can be tailored to have a specific spectral-power distribution at each frequency band of interest. As a consequence, the system impedances can be accurately measured over a wide frequency band. The performance of the method is verified through experimental measurements of a 2.7 kW grid-connected system, where grid impedance measurements and terminal inverter output admittance measurements are performed.

INDEX TERMS Impedance measurement, System identification, Broadband perturbation, Orthogonal sequences.

I. INTRODUCTION

THE rapid increase in grid-connected power electronics has disrupted the dynamics of most power systems and exposed challenges in the system compatibility and stability [1]. The detailed structure of the power system is often unknown, and the precise internal dynamics of commercial devices are often protected by the manufacturer. Consequently, impedance measurements are often the only option to identify the system dynamics. Recently, the impedance measurements have been applied for many purposes, such as stability analysis [2]–[6], controller design [7], and adaptive control [8]–[10].

Past studies have presented various measurement techniques to obtain the terminal impedance of the grid or grid-connected subsystem [2]–[4], [9], [11]. Particularly, broadband methods have become popular due to short measurement time where a broadband perturbation such as a pseudo-

random sequence (PRS) or an impulse is placed, for example, on top of the system's controller reference signal [9], [12]–[19]. The resulting responses in the system output voltages and currents are measured, and Fourier techniques are applied to extract the impedance information.

One of the most widely applied broadband sequence has been the maximum-length binary sequence (MLBS) which can be easily implemented, as the sequence has only two signal levels [20]. The MLBS exhibits multiple desirable characteristics, such as controllable frequency bandwidth and resolution, and low crest factor [21]. However, the MLBS suffers from very limited number of available signal lengths, as the sequence length is defined as $2^n - 1$ where n is a positive integer [21]. In addition, the spectral power of the MLBS is linearly distributed over many harmonic frequencies, which causes challenges in the identification of wide frequency bands where both the high- and low-frequency

characteristics are important to be measured. In many grid-connected systems, especially the low-frequency impedance (admittance) can be small resulting in a very weak response to the applied perturbation. Such systems include inductive transmission grids [22] and converter systems where control loops shape the terminal characteristics [23]. In order to increase the signal-to-noise ratio, either the injection amplitude has to be increased or more injection periods have to be applied and averaged to reduce the effect of noise. Both methods may become difficult in practice; increasing the amplitude may drift the system out of its linear region or disturb the normal operation of the system, whereas increasing the injection periods requires more computing power and memory storage [24].

Recent studies have presented perturbation signals that have adjustable spectral energies at specific frequency ranges. The authors in [24] applied the discrete-interval binary sequence (DIBS). The DIBS is a computer-optimized binary signal, where the goal of the optimization is to force as much power as possible into the specified (user-defined) harmonic frequencies without increasing the signal time-domain amplitude. In the DIBS, however, a significant amount of the signal total power appears in non-specified harmonics [21]. In addition, the iterative sequence design through computer optimization can be very complex. Another solution would be using a multi-sine perturbation, where multiple sinusoids with different frequencies are summed up [25]–[27]. However, the multi-sine typically has a large number of signal levels making it difficult to implement the signal with a low-cost application [24]. In addition, the multi-sine often exhibits large signal peaks in its time-domain waveform, making it unsuitable for sensitive systems [28]. The multisine crest factor can be minimized by phase optimization algorithms, such as in [29], however, these processes require high computational effort and affect the magnitude spectrum.

This work proposes a novel perturbation-design method to overcome the drawbacks of the MLBS. The proposed method is based on combined sequences where several orthogonal binary sequences are designed and summed up to form a single perturbation. The orthogonal sequences do not have power at common frequencies, and therefore, it is possible to independently design each sequence in the summation so that the spectral power of the sequences is distributed into specific frequency ranges. Summing up the sequences produces a near-binary signal which has a high degree of freedom in terms of signal length and spectral power distribution compared to the MLBS. As a result, the frequency-specific excitation power can be drastically increased without increasing the signal time-domain amplitude, and the system impedance(s) can be measured significantly more accurately compared to a similar-amplitude MLBS. In addition, as the frequency resolution of each orthogonal sequence in the combined signal can be separately selected, one can adjust the resolution to a very fine value within a specific frequency range so that possible resonances can be accurately measured. Otherwise the produced signal has the same attractive
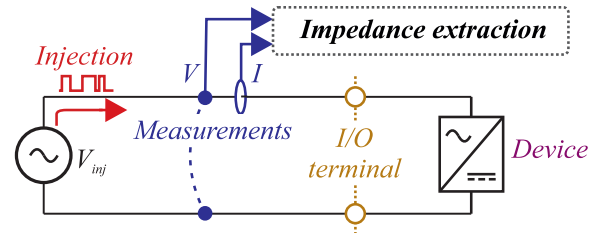

FIGURE 1. Schematic of a converter terminal impedance measurement.

properties than the conventional MLBS.

The remainder of the work is organized as follows. Section II reviews the theoretical background for impedance measurements using pseudo-random sequences. Section III presents the proposed design method for multiple orthogonal sequences. Section IV presents experimental validation based on a 2.7 kW three-phase grid-connected inverter system. Section V concludes the work.

II. IMPEDANCE MEASUREMENTS WITH PSEUDO-RANDOM SEQUENCES
A. MEASURING TERMINAL IMPEDANCE
Fig. 1 presents a simplified diagram of a typical broadband-measurement setup for a power-electronic device for obtaining the terminal impedance, where V_{inj} denotes the voltage injection and V and I are the measured terminal voltage and current. The perturbation is injected to the system as a voltage- or current-type excitation, for example by applying the current references of an inverter. The voltages and currents are measured, and transformed to the frequency domain through discrete Fourier transformation (DFT)

$$\hat{X}(j\omega) = \mathcal{F}\{\hat{x}(t)\} \tag{1}$$

where $\hat{x}(t)$ is a measured time-domain signal and $\hat{X}(j\omega)$ is the corresponding frequency-domain signal. The frequency response (impedance or admittance) can be extracted from the frequency-domain input and output signals [14]

$$G(j\omega) = \frac{\hat{Y}(j\omega)}{\hat{X}(j\omega)} \tag{2}$$

where $\hat{X}(j\omega)$ is the input signal and $\hat{Y}(j\omega)$ is the output signal.

In three-phase AC systems, the impedance measurements are typically performed in the dq-domain, where the system can be transformed from time-periodic AC trajectories to time-invariant DC operating points [30]. However, the system becomes a multivariable system with two input signals and two output signals which are coupled through cross-coupling elements. To address this coupling effect in the impedance measurements, two independent sets of measurements are required [31], [32]. The complete impedance matrix can be obtained from

$$\begin{bmatrix} Z_d & Z_{qd} \\ Z_{dq} & Z_q \end{bmatrix} = \begin{bmatrix} V_{d1} & V_{d2} \\ V_{q1} & V_{q2} \end{bmatrix} \begin{bmatrix} I_{d1} & I_{d2} \\ I_{q1} & I_{q2} \end{bmatrix}^{-1} \tag{3}$$

where subscripts "1" and "2" are the two independent measurements. The independent measurements can be performed by, for example, sequentially injecting the perturbation to first d-channel and then to q-channel.

B. MAXIMUM-LENGTH BINARY SEQUENCE

Maximum-length binary sequence (MLBS) is a class of pseudo-random signals that can be straightforwardly generated using shift registers [20]. The MLBS is a periodic and deterministic binary sequence that exists for sequence lengths of $N = 2^n - 1$, where n is an integer larger than 2. Because the MLBS has only two different signal levels, the sequence is easy to generate in low-cost hardware. The frequency spectrum of the MLBS is linearly spaced with a resolution of $f_{\mathrm{res}} = f_{\mathrm{gen}}/N$, where f_{gen} is the signal generation frequency. The measurement duration of a single period is $T_{\mathrm{m}} = 1/f_{\mathrm{res}}$, and due to the signal periodicity, the MLBS can be averaged over multiple periods to increase the signal-to-noise ratio.

C. ORTHOGONAL SEQUENCES

Orthogonal sequences are signals that are uncorrelated with each other, that is, they have no power at same frequencies. Such sequences have been typically applied in systems that have multiple inputs and outputs. Using the orthogonal sequences as injections makes it possible to simultaneously measure the frequency responses between several (coupled) inputs and outputs [4]. In the present work, however, the orthogonal sequences are applied to form a single perturbation sequence.

Various techniques have been presented to implement orthogonal broadband sequences. One of the most common approach is the use of Hadamard modulation [21], where the conventional MLBS is used as a first sequence. The second (orthogonal) sequence is formed by modulating the MLBS with a 2-bit sequence [0 1], which results in a sequence whose length is doubled and all the even-order harmonics are suppressed. Similarly, the third sequence is formed by modulating the MLBS with a sequence [0 0 1 1]. Further orthogonal sequences can be formed by continuing this modulation pattern for an arbitrary number of sequences. Detailed instructions for applying the modulation can be found in [21]. Fig. 2 presents three orthogonal binary sequences in the frequency domain, generated by the Hadamard modulation. The sequences have different amplitudes for illustration, they are generated at 1 kHz and have lengths of 31 for sequence 1, 62 for sequence 2, and 124 for sequence 3. As the figure shows, the sequences have no power at common frequencies.

III. COMBINING MULTIPLE ORTHOGONAL SEQUENCES

This work proposes a novel application for orthogonal sequences; a combined orthogonal sequence (COS) is generated by summing up multiple orthogonal binary sequences (OBS). This provides added degrees of freedom in the perturbation design as each of the orthogonal sequences can be independently designed for a specific frequency range. The COS is a near-binary sequence in which the spectral power is
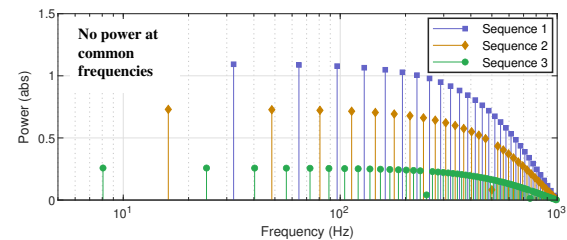

FIGURE 2. Power spectra of three orthogonal sequences.

significantly increased at specific frequency ranges compared to the MLBS. Additionally, the frequency resolution of the produced sequence can be selected differently for specific frequency ranges thus enabling accurate evaluation of, for example, resonance peaks.

A. DESIGNING THE COS

The COS can be designed by using the following steps (an example by using three orthogonal sequences)

1) Design an MLBS so that the generation frequency is twice higher than highest frequency to be identified, and choose the sequence length so that a sufficient frequency resolution is achieved for the high-frequency range.
2) Produce a second orthogonal sequence from the MLBS, and choose a lower generation frequency to target the middle-range frequencies.
3) Produce a third orthogonal sequence and choose even lower generation frequency to target the low-frequency range.
4) Choose the excitation amplitude for each sequence.
5) Combine the sequences by summing them together.

In order to preserve the orthogonality of the sequences, the generation frequencies must be integer multiples of each other, and each new sequence must have lower generation frequency compared to the previous sequence. The measurement duration of the COS is determined by the sequence that has the lowest generation frequency (the last OBS). The other OBS, which have shorter duration for a single period, occur multiple periods within the total duration. As a consequence, each individual sequence is applied with integer number of periods and the sequence periodicity is preserved.

The impedance calculation through Fourier methods is straightforward and two approaches exist. The first approach is to calculate a separate discrete Fourier transformation (DFT) for each of the OBS, where the impedance can be obtained similarly than in conventional broadband sequence analysis. However, this approach requires the use of multiple DFTs, which may increase the required calculation power. Alternatively, a single DFT can be performed and the analysis is performed by the following steps:

1) Inject h orthogonal sequences to the system (OBS$_1$, OBS$_2$, ... ,OBS$_h$) at corresponding generation frequen-

cies $f_{\text{gen}}^1, f_{\text{gen}}^2, .., f_{\text{gen}}^{\text{h}}$ (at a descending order). Measure the input and output signals.

2) Perform a k-point DFT on the signals, where $k = n * f_{\text{s}}/f_{\text{gen}}^{\text{h}}$, where f_{s} is the sampling frequency and n is the length of the highest order OBS that is generated at the lowest frequency.

3) For the last orthogonal sequence (OBS$_{\text{h}}$), select the harmonics that satisfy

$$(i - 1) \bmod 2 = 0 \tag{4}$$

where i is the order of the harmonic.

4) For the first orthogonal sequence (OBS$_1$), select the harmonics that satisfy

$$(i - 4 * f_{\text{gen}}^1/f_{\text{gen}}^{\text{h}}) \bmod (4 * f_{\text{gen}}^1/f_{\text{gen}}^{\text{h}}) = 0 \tag{5}$$

5) For the remaining orthogonal sequences, select the harmonics that satisfy

$$(i - 2 * f_{\text{gen}}^j/f_{\text{gen}}^{\text{h}}) \bmod (4 * f_{\text{gen}}^j/f_{\text{gen}}^{\text{h}}) = 0 \tag{6}$$

where j is the order of the OBS in the range from 2 to $h - 1$

6) For each OBS, remove the harmonics that are above 60.3 % of the corresponding generation frequency (a 6 dB decrease in the excitation amplitude).

This procedure selects the excited frequencies from the spectrum, and the impedance can be obtained from the output-to-input ratio.

The major benefit of the proposed COS is that the perturbation can be flexibly optimized to extract information from systems that are challenging to measure with conventional MLBS. Therefore, the optimal design of the COS is case dependent. In general, the generation frequency of the first sequence (that is, the base MLBS) can be designed similarly than when a single MLBS is applied; the generation frequency should be twice the highest frequency-of-interest, as the measurement bandwidth is limited to half of the generation frequency. However, the length of the first sequence is chosen so that the resolution in the high-frequency range is sufficient, in contrast to conventional approach with a single MLBS where the frequency resolution must satisfy also the low-frequency-range requirements. Then, additional OBS can be added (with respect to design rules in the steps above) to reinforce the perturbation at specific frequency ranges, for example by enhancing the frequency resolution at the low-frequency range. The amplitude of the COS, which is the summation of OBS amplitudes, should be designed similarly than the amplitude of a single MLBS injection which is discussed in [33]. The amplitudes of individual OBS should be chosen so that the frequency ranges that have the lowest frequency-response magnitude or the highest noise content should have the highest amplitude.

B. EXAMPLE IMPLEMENTATION OF COS

Fig. 3 presents an implementation of the proposed method for three orthogonal sequences that are generated with different
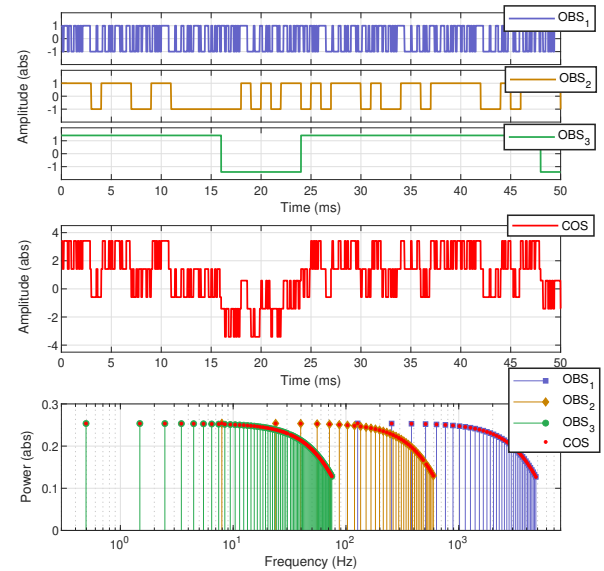

FIGURE 3. Three orthogonal sequences in the time and frequency domain.
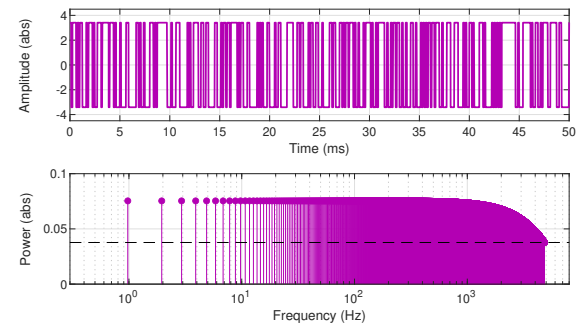

FIGURE 4. Conventional 8191-bit-long MLBS.

frequencies. The OBS have sequence lengths of 63, 126, and 252, while the respective generation frequencies are 8000 Hz, 1000 Hz, and 125 Hz. The COS shown in red is obtained by summing up the three orthogonal sequences. The orthogonality is preserved as seen from the spectral lines that never occur at the same frequency. A -6 dB is considered to be the threshold for excitation power, below which the excitation power is insufficient and ignored. The COS has a relatively low number of different signal levels (two times the number of the applied orthogonal sequences) making it straightforward to be generated even with a low-cost controller. The sequence is periodic and can be averaged over multiple periods to increase the signal-to-noise ratio. The measurement duration is determined by the length and generation frequency of the longest sequences, similarly than with a single MLBS.

Fig. 4 shows a conventional MLBS for a comparison to the combined sequence. The MLBS is designed so that the injection amplitude and resolution at low frequencies are equal to the combined sequence, so a 8191-bit-long MLBS
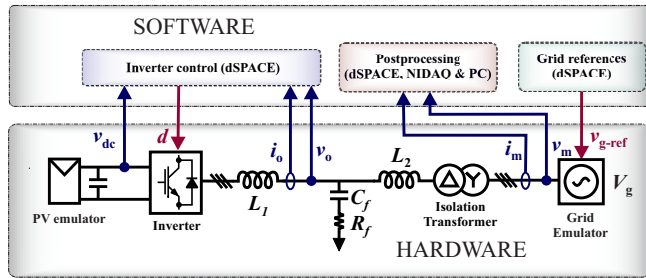
FIGURE 5. Experimental setup for impedance measurements.
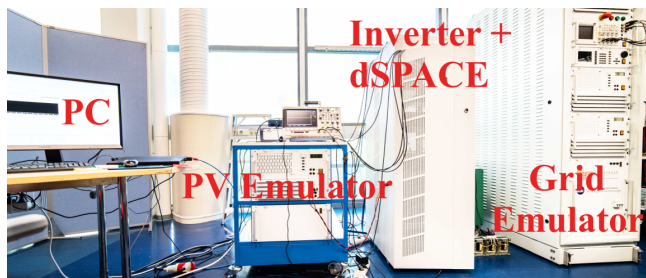

FIGURE 6. Photograph of the experimental setup.

generated at 8 kHz is applied. While the maximum amplitude is equal in both sequences, the combined sequence has lower total power as the time-domain signal includes levels below the maximum amplitude. Therefore, the combined sequence produces less disturbances to the measured system. Despite the lower total power, the COS has up to 230 % more excitation power on each frequency harmonic due to lower total number of spectral power harmonics, which is the main advantage of the proposed sequence.

IV. EXPERIMENTS

Fig. 5 shows the experimental setup that is used to perform the measurements, and a photograph of the setup is shown in Fig. 6. A four-quadrant linear amplifier (*Spitzenberger Spies PAC 15000*) is set to emulate the grid voltages for a grid-connected three-phase inverter (*Myway Plus MWINV-9R144*). The inverter control system is implemented in a dSPACE real-time simulator, and the DC power is provided by a photovoltaic emulator (*Spitzenberger Spies PVS 7000*). An external CL-filter and isolation transformer are used to interface the inverter to the grid. In the grid impedance measurements, an additional inductor is connected between the transformer and the grid to emulate the grid impedance. The setup parameters are shown in Table 1.

Fig. 7 presents the detailed schematics of the subsystems that control the devices and perform the postprocessing. The inverter is operated in a cascaded control scheme, where the outer DC voltage controller is responsible for the DC voltage control of the DC link that connects the inverter to the PV emulator. The innermost current controller controls the output currents, where the reference for the d-component is the output of the outer voltage controller and the q-component
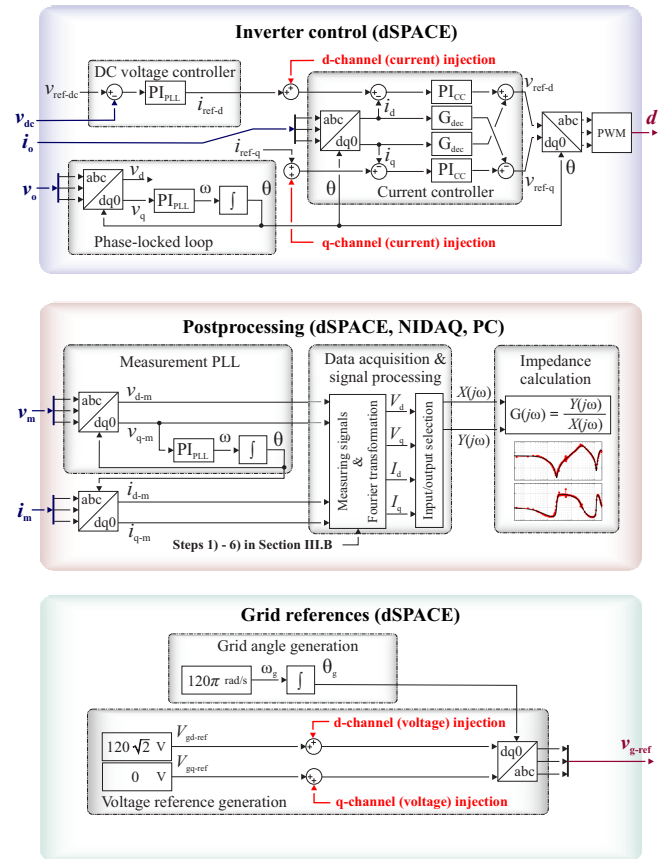

FIGURE 7. Detailed schematics of the control and postprocessing blocks.

reference is set to zero (that is, the inverter operates at unity power factor). The voltage references for the grid emulator are also formed in the dq-domain. The perturbation signal can be injected to either inverter current controller (d- or q-channel) or the grid voltage references (d- or q-channel). Consequently, the configuration enables impedance measurement on any of the impedance component for the inverter or the grid. Moreover, the complete 2x2 matrices can be extracted for both subsystems by applying four sequential measurements and applying Eq. (3). In the postprocessing, the measured signals are transformed into dq-domain by an additional low-bandwidth phase-locked loop.

The effectiveness of the proposed method is demonstrated by performing grid impedance measurements and output terminal admittance measurements on a grid-connected inverter. The measurements are performed both with the proposed COS and conventional MLBS. Both sequences are designed so that they have approximately the same time-domain amplitude, measurement duration, measurement bandwidth, and low-frequency frequency resolution. In the first set, the grid impedance is measured by utilizing the inverter in the current-type excitation injection. In the second set, a voltage-type injection from the grid emulator is applied in the measurements of inverter's output admittance. The measurements are performed in the dq-domain for the impedance

TABLE 1. Parameters of the experimental setup.

Parameter	Symbol	Value
Grid frequency	f_n	60 Hz
Grid phase voltage	V_g	120 V
Inverter nominal power	S_n	2.7 kVA
Switching frequency	f_{sw}	8 kHz
Power factor	$\cos\phi$	1.0
Switching deadtime	T_{dt}	4.0 μs
DC voltage	V_{dc}	414.3 V
DC input current	I_{dc}	6.577 A
DC capacitor capacitance	C_{dc}	1.5 mF
L-filter inductance	L_1	2.2 mH
L-filter resistance	R_1	100 mΩ
CL-filter inductance	L_2	0.6 mH
CL-filter resistance	R_2	40 mΩ
CL-filter capacitance	C_f	10 μF
CL-filter damping resistance	R_d	1.8 Ω
Transformer inductance	L_{tf}	0.3 mH
Transformer resistance	R_{tf}	400 mΩ
Additional inductance	L_g	4 mH
Additional resistance	R_g	100 mΩ
AC current control proportional gain	$K_{P\text{-}CC}$	0.0149
AC current control integral gain	$K_{I\text{-}CC}$	23.442
DC voltage control proportional gain	$K_{P\text{-}VC}$	0.0962
DC voltage control integral gain	$K_{I\text{-}VC}$	1.2092
PLL control proportional gain	$K_{P\text{-}PLL}$	2.3280
PLL control integral gain	$K_{I\text{-}PLL}$	351.720

FIGURE 8. Schematic of the grid impedance measurements.

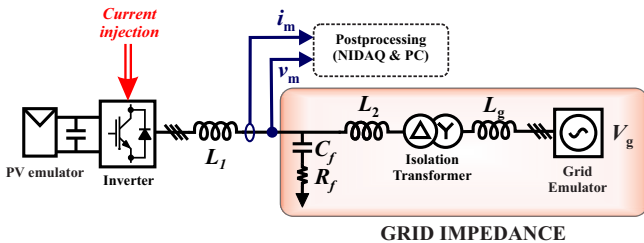**FIGURE 9.** Time domain waveform and frequency domain spectrum for the MLBS (purple) and the COS (red) in grid impedance measurement.

d component. Finally, the complete 2x2 impedance matrices are measured for both the inverter and the grid, and an impedance-based stability analysis is performed.

A. GRID IMPEDANCE MEASUREMENTS

In the first experiment set, the three-phase inverter is utilized in the grid impedance measurement of the interfacing system. Fig. 8 presents a simplified schematic of the experiment, where the interfacing impedance consists of an external CL-filter, an isolation transformer, and an additional inductor that emulates the grid impedance. The perturbation signal is injected to the current references of the inverter resulting in a current-type excitation to the system. The inverter operates at the nominal setpoint feeding 2.7 kW to the grid, and the perturbation is superimposed to the fundamental current. The three-phase voltages and currents are measured at the grid interface and transformed to the dq-domain. Then, the signals are Fourier transformed and the impedance is obtained from the ratio of voltage and current.

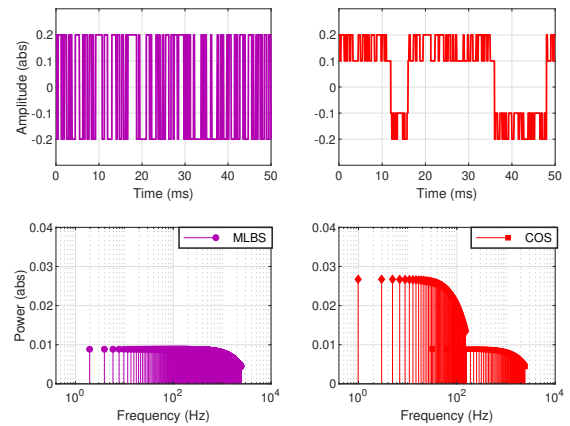The grid impedance measurements are performed by ap-

plying both the conventional MLBS and the COS. The perturbations are designed to have an equal bandwidth, measurement duration (T_m), and time-domain amplitude (A). In addition, the low-frequency resolution (f_{res}) is set to be equal. Due to characteristics of orthogonal sequences in COS, the MLBS is averaged over two periods to achieve equal measurement duration. The signal parameters are summarized in Table 2, where the number of averaged periods is denoted by P. The proposed COS is formed by summing up the two OBS. To improve the measurement performance at low frequencies, the COS design is weighted towards the low-frequency range by increasing the amplitude of the second OBS and simultaneously decreasing the amplitude of the first OBS.

Fig. 9 shows the time-domain waveforms and frequency spectra of the MLBS and the COS. Despite the equal total amplitude, the COS is designed to have significantly higher power in the low-frequency range to tackle the challenges related to the weak voltage response in low frequencies of an inductive grid. The injection amplitude is set to 0.2 A, which is approximately 2 % of the nominal current (10 A). The phase currents at the inverter point-of-common-coupling (PCC) are shown without perturbation and with the MLBS and COS perturbations in Fig. 10. Fig. 11 presents the PCC voltages showing that the injection has a very small effect on the voltages. The disturbance from the excitation to the fundamental currents and voltages is negligible, which makes the perturbations highly suitable in, for example, online identification of grid-connected systems.

Fig. 12 shows the measured grid impedance by applying

TABLE 2. Sequence parameters for grid-impedance measurements.

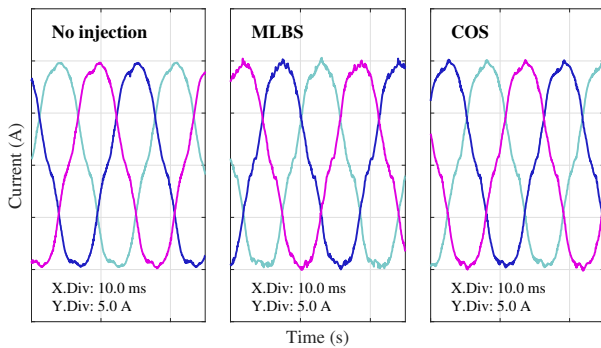|	N	f_{gen} (Hz)	A (A)	f_{res} (Hz)	P	T_m (s)
OBS$_1$	127	4000	0.05	31.5	32	1.016
OBS$_2$	254	250	0.15	1.97	1	1.016
COS	381	250..4000	0.2	1.97..31.5	1	1.016
MLBS	2047	4000	0.2	1.95	2	1.024

FIGURE 10. Phase currents without injection and with MLBS and COS perturbation.
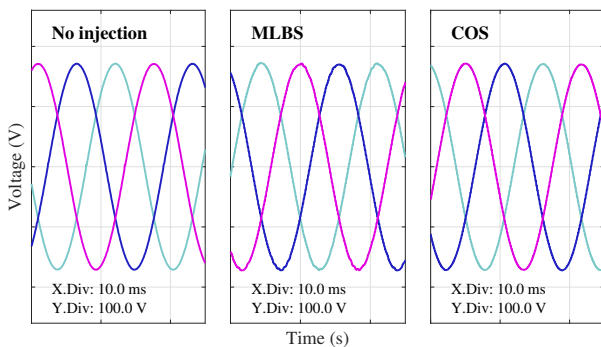

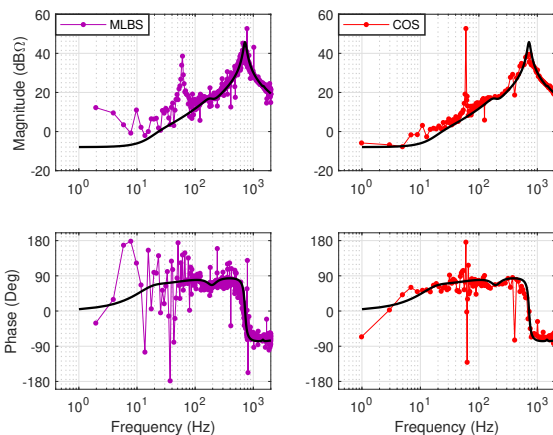FIGURE 11. Phase voltages without injection and with MLBS and COS perturbation.

FIGURE 12. Grid impedance measurements by applying the MLBS (purple) and the COS (red).

both the MLBS and the COS. The COS demonstrates drastically improved accuracy resulting from the higher frequency-specific excitation power, especially in the low-frequency range. With the COS, also the high-frequency resonant peak is still adequately identified, despite the lower frequency resolution at these frequencies. On the other hand, similar low-frequency resolution to the MLBS ensures that the low-
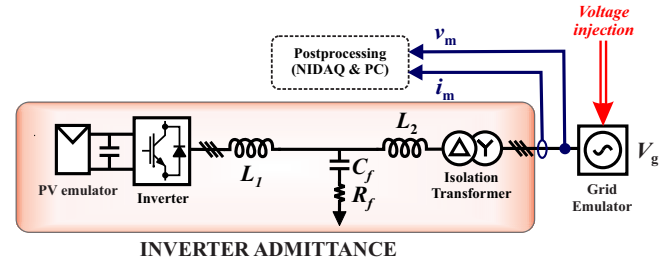

FIGURE 13. Schematic of the inverter terminal admittance measurements.

frequency dynamics are accurately captured. As both the injection amplitude and measurement duration are chosen very small for both perturbations, the measurement accuracy is adversely affected. The accuracy could be increased by increasing either the injection amplitude or measurement duration. However, this trade-off is not possible in some applications where fast measurements of sensitive systems are required. By applying the the proposed combined orthogonal sequences, the accuracy can be improved without increasing the duration or injection amplitude.

B. INVERTER OUTPUT ADMITTANCE MEASUREMENTS

In the second experiment set, the total terminal admittance of the inverter, filter, and transformer is measured as seen from the grid-side. Fig. 13 presents the measurement configuration for inverter admittance measurements. The measurements are performed with a voltage-type injection by superimposing the perturbation signal to the grid voltages through the grid emulator. The measurements are performed both by the COS and the conventional MLBS. The inverter admittance is expected to have multiple resonant peaks resulting from the controllers and LCL-interactions, and the inverter admittance measurements at low frequencies typically requires a relatively high SNR compared to higher frequencies. Consequently, the COS is designed to consist of three orthogonal sequences. The signal parameters are summarized in Table 3. As the third orthogonal sequence (OBS_3) covers the low-frequency region, the injection amplitude is set to a higher value compared to the other two sequences. Fig. 14 presents the time-domain waveforms and power spectra of the applied perturbations. As the figure shows, the combined sequence can be designed to have a significantly higher spectral power at specific frequencies compared to the MLBS when the time-domain amplitudes are similar.

Fig. 15 shows the measured output admittance of the inverter when both the MLBS and the proposed perturbation

TABLE 3. Sequence parameters for inverter measurements.

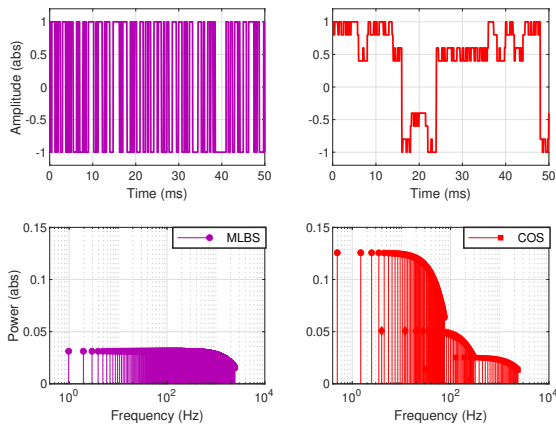|	N	f_{gen} (Hz)	A (V)	f_{res} (Hz)	P	T_m (s)
OBS_1	63	4000	0.1	63.5	128	2.016
OBS_2	126	500	0.2	7.94	8	2.016
OBS_3	252	125	0.7	0.99	1	2.016
COS	411	125..4000	1	0.99..64	1	2.016
MLBS	4095	4000	1	0.98	2	2.048

FIGURE 14. Time domain waveform and frequency domain spectrum for the MLBS (purple) and the COS (red).
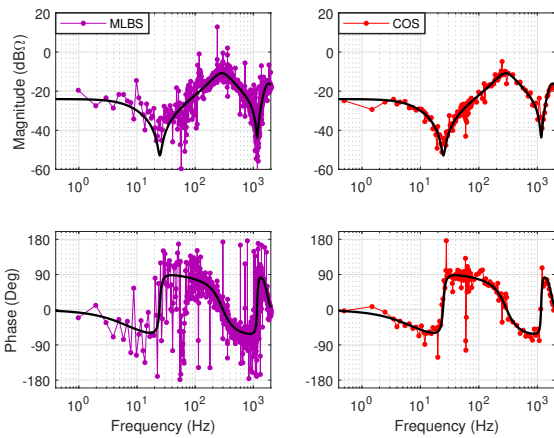

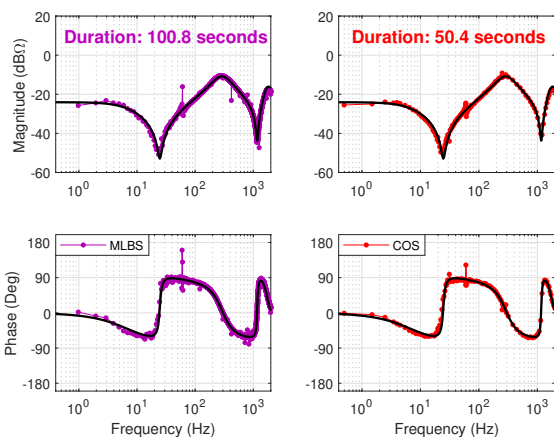**FIGURE 15.** Admittance measurements by applying the MLBS (purple) and the COS (red).

FIGURE 16. Long-duration admittance measurements by applying 100 periods of the MLBS (purple) and 25 periods of the COS (red).
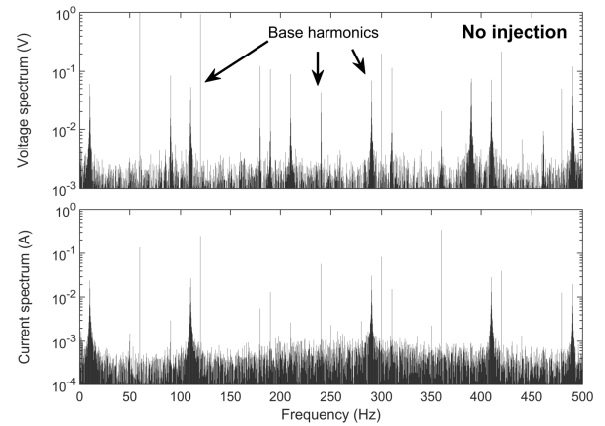

FIGURE 17. Spectra of d-channel voltages and current with no injection.

is applied (the analytically obtained admittance is shown as a reference). The figure shows the superiority of the combined sequence compared to the MLBS, as the measurement obtained by the combined sequence follows the reference much more accurately through the whole frequency band, including the resonant peaks. With the combined sequence, the SNR can be increased to overcome the effects of noise, harmonic currents, and nonlinearities that corrupt the MLBS measurement.

The measurement results can be further improved by averaging the results over multiple injection periods. Fig. 16 presents long-duration measurements of the output admittance of the inverter, where the MLBS has bee applied with 100 periods and the COS with 25 periods. The durations of the measurements are 100.8 s and 50.4 s, respectively. As the figure shows, similar (or even better) accuracy can be achieved in significantly shorter measurement duration when the proposed COS is applied. Consequently, the proposed method can also be applied to reduce the measurement duration in applications where a high accuracy is required, such as stability analysis of grid-connected systems.

C. SPECTRAL ANALYSIS

In order to validate the superiority of the COS, a spectral analysis is performed to show the effect of the applied perturbation in the measured voltages and currents. Fig. 17 shows the d-component voltage and current spectra in the nominal operation conditions when no injection is applied. In the phase-domain, the current harmonics have magnitudes of 1.2 % for the 3rd harmonic, 5.4 % for the 5th harmonic, and 2.0 % for the 7th harmonic. However, in the dq-frame the harmonics are shifted by the fundamental frequency $\pm f_n$ due to rotating reference frame. The harmonic currents result mostly from the inverter switching and system nonlinearities, such as saturation in the isolation transformer. The inverter switches have a high deadtime of $4\ \mu s$ with respect to the 8 kHz switching frequency degrading the current quality.

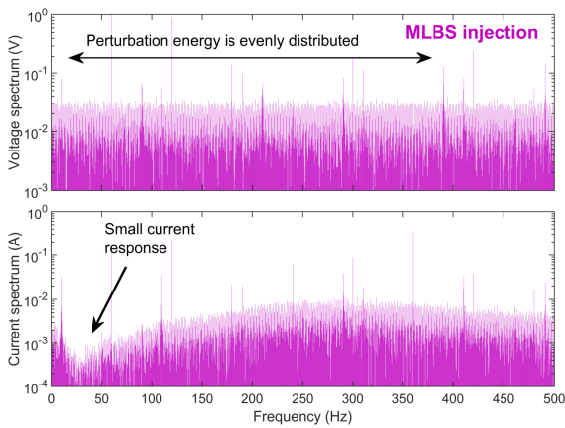Fig. 18 shows the corresponding spectra when the voltage-

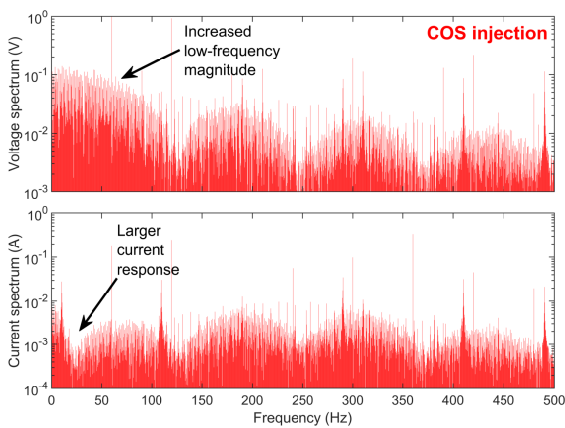**FIGURE 18.** Spectra of d-channel voltages and current with the MLBS.

FIGURE 19. Spectra of d-channel voltages and current with the COS.

type MLBS perturbation applied in the inverter output admittance measurements is injected to the grid voltages. The excited frequencies at the voltage spectrum have an even power distribution. At the low-frequency anti-resonance, however, the current response is very small drastically degrading the measurement performance. Fig. 19 shows the corresponding spectra when the proposed COS is injected. With the COS, the excitation spectrum is weighted towards the low frequencies in the perturbation design. Consequently, also the current response spectrum is enhanced at the critical frequencies.

Fig. 20 shows the low-frequency spectra for both perturbation signals, where the excited frequencies have been highlighted. The comparison between the inherent noise and excited frequencies when both the MLBS and the COS are applied explains the superior performance of the COS. The adjustable amplitude spectrum of the COS allows improving the SNR at certain frequency ranges. In this case, the admittance at the anti-resonant peak is approximately -50 dBΩ, so the current response is only 0.3 % of the voltage excitation. Therefore, enhancing the excitation amplitude near these frequencies is critical for high-performance measurements.
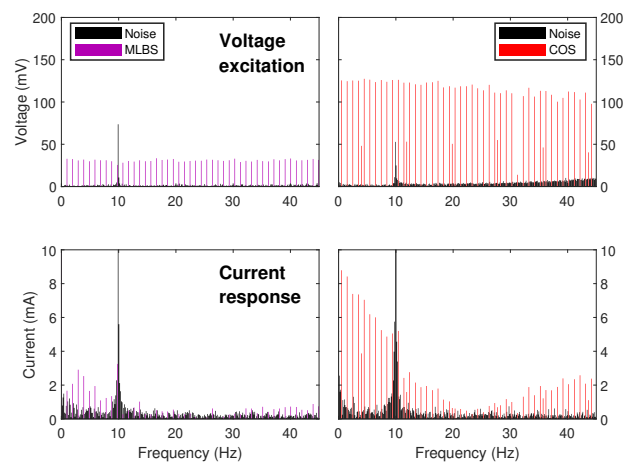

FIGURE 20. Low-frequency current and voltage spectra for the MLBS and the COS injection with highlight on excited frequencies.

TABLE 4. Total harmonic distortions in phase currents and voltages.

	Voltage THD	Current THD
No excitation	0.3 %	6.47 %
MLBS excitation	0.54 %	6.91 %
COS excitation	0.45 %	6.60 %

In order to quantify the disturbance of the perturbation injection for the system operation, the total harmonic distortions (THDs) are measured. The phase current and voltage THDs are shown in Table 4 for the three cases. As the excitation amplitude is chosen small, the perturbation has only a minor impact on the THDs, as the base level without perturbations is close to the THD during the measurements. Although the impact is low for both perturbation signals, the COS disturbs the system even less than the MLBS.
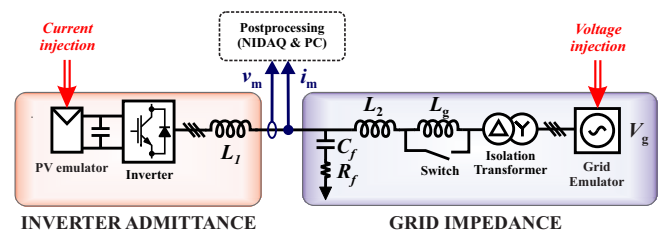

FIGURE 21. Measurement setup diagram for the stability analysis.

D. STABILITY ANALYSIS
The stability analysis of grid-connected devices is a common utilization for the impedance measurements [34], [35]. In this section, an impedance-based stability analysis is performed by applying the impedance measurements obtained with the COS and the MLBS. Multivariable impedances (2x2 matrix in dq-domain) are obtained by two independent measurements where the perturbation is first injected to the d-channel and then to the q-channel and applying Eq. (3). The stability
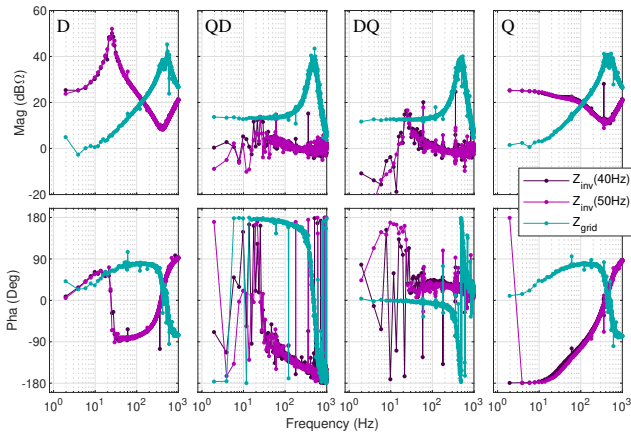
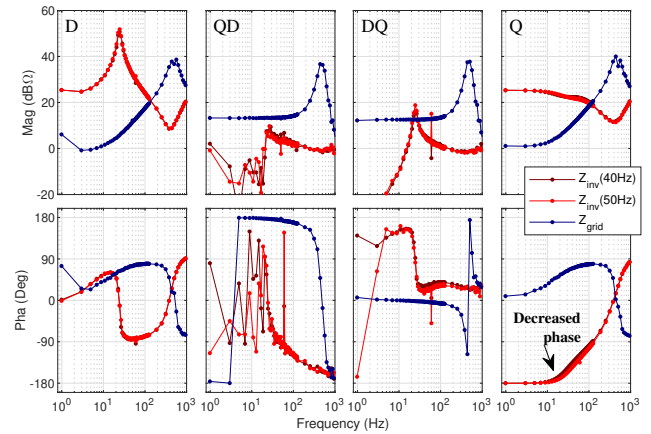**FIGURE 22.** Complete impedance matrices measured with the MLBS.

FIGURE 23. Complete impedance matrices measured with the COS.

experiments are performed with a 9 mH inductor as the grid impedance and by tuning the bandwidth of the inverter's phase-locked loop, as the high PLL bandwidth is known to deteriorate system stability [23]. The setup configuration is shown in Fig. 21 and the stability analysis is performed as follows

1) The PLL is set to very low bandwidth (1 Hz) and the grid impedance measurements are performed by applying current injection from the inverter
2) The grid impedance is disconnected, and the inverter output admittance is measured for two sets of PLL parameters (40 Hz and 50 Hz) by applying voltage injection from the inverter
3) The multivariable impedances are calculated for each measurement set and the stability analysis is performed by assessing the impedance ratio of the grid and the inverter (for both PLL parameter sets).

The measurements are performed both by MLBS and COS, and the obtained results are compared. The PLL controller parameters are shown in Table 5.

TABLE 5. Phase-locked loop parameters for the stability experiments.

Bandwidth	Proportional gain	Integral gain
1 Hz	0.0388	0.0977
40 Hz	1.5520	156.32
50 Hz	1.9400	244.25

Performing the stability analysis relies on the impedance ratio of the subsystems, and consequently, both the subsystems must be measured at the same frequencies. Therefore, the measurements are performed with the same COS design for both the grid and the inverter. The sequence designed for the grid impedance measurements is selected and also the MLBS is designed similarly (Table 2). The total injection amplitude is set to 0.2 A for current injection and 2 V for voltage injection. The measurements are averaged over 50 periods for the COS and 100 periods for the MLBS, and the
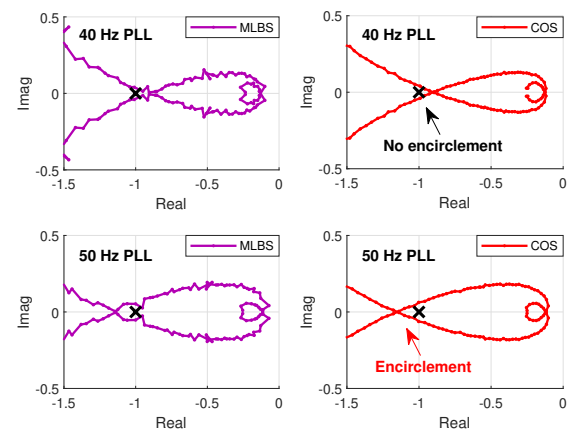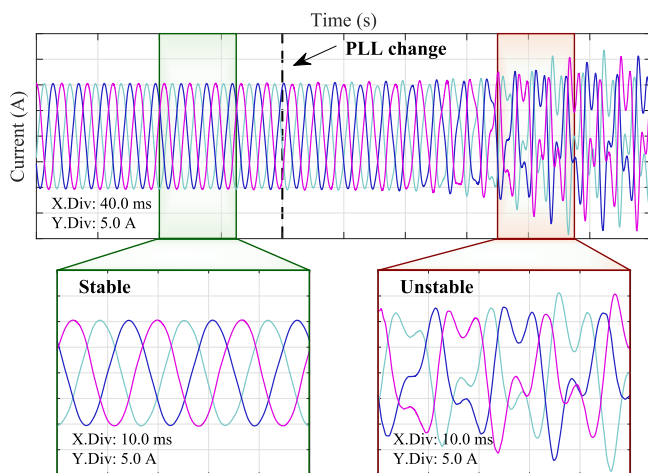

FIGURE 24. Nyquist loci of the 40 Hz (upper) and 50 Hz (lower) PLL systems measured with MLBS (purple) and COS (red).

total measurement duration for each set of measurements is 51 seconds.

Fig. 22 presents the measured impedance matrix of the grid impedance and inverter output impedance (shown as impedance instead of admittance) measured by applying the MLBS. In Fig. 23, the impedances measured with the COS are shown. It should be noted that the change in PLL bandwidth has only a minor impact on the impedances besides the phase decrease in the q-channel impedance. In order to assess the system stability, the generalized Nyquist criterion is applied to the impedance ratio [36]. Fig. 24 presents the eigenloci for both system configurations (40 Hz and 50 Hz PLL bandwidth) measured with both the MLBS and the COS. As seen from the figure, both measurements indicate stability for the 40 Hz PLL and instability for the 50 Hz PLL (as the locus encircles the critical point). The measurements with COS show superior accuracy over the MLBS.

In order to validate the predicted system stability, an experiment is performed where the PLL controller bandwidth

This article has been accepted for publication in a future issue of this journal, but has not been fully edited. Content may change prior to final publication. Citation information: DOI 10.1109/ACCESS.2020.3026727, IEEE Access

Alenius *et al.*: Combination of Orthogonal Injections in Impedance Measurements

FIGURE 25. Three-phase currents when the PLL bandwidth is increased from 40 Hz to 50 Hz and the stability is lost.

is abruptly changed from 40 Hz to 50 Hz by changing the controller gains. Fig. 25 presents the three-phase current waveforms measured from the grid. In prior to changing the PLL bandwidth, the current waveforms are smooth and sinusoidal. However, increasing the PLL bandwidth provokes an increasing oscillation to the currents, which indicates an unstable system. This experiment validates the performed stability analysis.

V. CONCLUSION

Impedance measurements are important in the design and analysis of power-electric systems. Recently, significant research effort has been directed to the design of perturbation sequences, as the measurement quality is strongly dependent on the applied perturbation signal. Pseudo-random broadband sequences have demonstrated multiple desirable characteristics, but the linear power distribution of those sequences causes challenges especially in systems that have a wide frequency-range of interest. This work proposed a novel method for the perturbation design. In the method, multiple orthogonal binary sequences are summed up forming a near-binary signal. As the orthogonal sequences can be independently designed, the produced signal can have much higher power at certain frequency bands compared to the conventional MLBS with a similar time-domain amplitude. Additionally, the frequency resolution of the sequences can be selected differently, allowing sufficient resolution over a wide frequency range. Experimental measurements based on a grid-connected inverter system were presented to demonstrate the effectiveness of the proposed method. The results clearly showed the superiority of the proposed combined sequence compared to the conventional MLBS. An experimental stability analysis was performed based on the impedance measurements to present an example utilization for the measured impedances. It is also emphasized, that the proposed method can be applied not only in grid-connected systems but in a wide range of systems where pseudo-random

sequences are used for system identification.

REFERENCES

[1] B. Bose, "Global Energy Scenario and Impact of Power Electronics in 21St. Century," IEEE Transactions on Industrial Electronics, vol. 60, no. 7, pp. 2638–2651, 2013.

[2] R. Luhtala, T. Roinila, and T. Messo, "Implementation of Real-Time Impedance-Based Stability Assessment of Grid-Connected Systems Using MIMO-Identification Techniques," IEEE Transactions on Industry Applications, vol. 54, no. 5, pp. 5054–5063, 2018.

[3] Y. Tang, R. Burgos, B. Wen, D. Boroyevich, J. Verhulst, D. Vrtachnik, and M. Belkhayat, "A Novel dq impedance measurement method in three-phase balanced systems," in 2019 IEEE 20th Workshop on Control and Modeling for Power Electronics, COMPEL 2019, 2019.

[4] T. Roinila, T. Messo, and E. Santi, "MIMO-identification techniques for rapid impedance-based stability assessment of three-phase systems in DQ Domain," IEEE Transactions on Power Electronics, vol. 33, no. 5, pp. 4015–4022, 2018.

[5] H. Alenius and T. Roinila, "Impedance-Based Stability Analysis of Paralleled Grid-Connected Rectifiers: Experimental Case Study in a Data Center," Energies, vol. 13, no. 2109, 2020.

[6] B. Wen, D. Boroyevich, R. Burgos, P. Mattavelli, and Z. Shen, "Small-Signal Stability Analysis of Three-Phase AC Systems in the Presence of Constant Power Loads Based on Measured d-q Frame Impedances," IEEE Transactions on Power Electronics, vol. 30, no. 10, pp. 5952–5963, 2015.

[7] T. Messo, A. Aapro, T. Suntio, and T. Roinila, "Design of grid-voltage feedforward to increase impedance of grid-connected three-phase inverters with LCL-filter," 2016 IEEE 8th International Power Electronics and Motion Control Conference, IPEMC-ECCE Asia 2016, pp. 2675–2682, 2016.

[8] R. Luhtala, T. Messo, and T. Roinila, "Adaptive Control of Grid-Voltage Feedforward for Grid-Connected Inverters based on Real-Time Identifications of System Stability Margins," in IPEC-Niigata 2018 -ECCE ASIA, 2018, pp. 1–8.

[9] A. Riccobono, M. Cupelli, A. Monti, E. Santi, T. Roinila, H. Abdollahi, S. Arrua, and R. A. Dougal, "Stability of shipboard dc power distribution: Online impedance-based systems methods," IEEE Electrification Magazine, vol. 5, no. 3, pp. 55–67, 2017.

[10] M. Cespedes and J. Sun, "Online grid impedance identification for adaptive control of grid-connected inverters," 2012 IEEE Energy Conversion Congress and Exposition, ECCE 2012, pp. 914–921, 2012.

[11] H. Alenius, T. Messo, T. Reinikka, and T. Roinila, "Aggregated Modeling and Power Hardware-in-the-Loop Emulation of Grid Impedance," in IEEE Energy Conversion Congress and Exposition 2018, 2018, pp. 4179–4186.

[12] R. Luhtala, H. Alenius, T. Messo, and T. Roinila, "Online Frequency Response Measurements of Grid-Connected Systems in Presence of Grid Harmonics and Unbalance," IEEE Transactions on Power Electronics, vol. 35, no. 4, pp. 3343–3347, 2020.

[13] T. Roinila and T. Messo, "Online Grid-Impedance Measurement Using Ternary-Sequence Injection," IEEE Transactions on Industry Applications, vol. 54, no. 5, pp. 5097–5103, 2018.

[14] T. Roinila, T. Messo, T. Suntio, and M. Vilkko, "Pseudo-Random Sequences in DQ-Domain Analysis of Feedforward Control in Grid-Connected Inverters," IFAC-PapersOnLine, vol. 48, no. 28, pp. 1301–1306, 2015. [Online]. Available: http://dx.doi.org/10.1016/j.ifacol.2015.12.311

[15] D. Martin, E. Santi, and A. Barkley, "Wide Bandwidth System Identification of AC System Impedances by Applying Pertubations to an Existing Converter," in 2011 IEEE Energy Conversion Congress and Exposition. IEEE, 2011, pp. 2549–2556.

[16] J. Siegers, E. Santi, and A. Barkley, "Wide bandwidth system identification of MVDC distribution system by applying perturbations to an existing converter," 2013 IEEE Electric Ship Technologies Symposium, ESTS 2013, pp. 434–441, 2013.

[17] A. Riccobono, M. Mirz, and A. Monti, "Noninvasive Online Parametric Identification of Three-Phase AC Power Impedances to Assess the Stability of Grid-Tied Power Electronic Inverters in LV Networks," IEEE Journal of Emerging and Selected Topics in Power Electronics, vol. 6, no. 2, pp. 629–647, 2018.

[18] J. Koppinen, J. Kukkola, and M. Hinkkanen, "Plug-In Identification Method for an LCL Filter of a Grid Converter," IEEE Transactions on Industrial Electronics, vol. 65, no. 8, pp. 6270–6280, 2018.

[19] H. Alenius, T. Roinila, R. Luhtala, T. Messo, A. Burstein, E. de Jong, and A. Fabian, "Hardware-in-the-Loop Methods for Stability Analysis of Multiple Parallel Inverters in Three-Phase AC Systems," IEEE Journal of Emerging and Selected Topics in Power Electronics, pp. 1–10, 2020. [Online]. Available: https://doi.org/10.1109/JESTPE.2020.3014665

[20] W. Davies, "Using the binary maximum length sequence for the identification of system dynamics," Proceedings of the Institution of Electrical Engineers, vol. 114, no. 10, p. 1582, 1967.

[21] A. H. Tan and K. Godfrey, Industrial Process Identification - Perturbation Signal Design and Applications, 1st ed. Springer, 2019.

[22] M. Liserre, R. Teodorescu, and F. Blaabjerg, "Stability of Photovoltaic and Wind Turbine Grid-Connected Inverters for a Large Set of Grid Impedance Values," IEEE Transactions on Power Electronics, vol. 21., no. No. 1, 2006.

[23] L. Harnefors, M. Bongiorno, and S. Lundberg, "Input-admittance calculation and shaping for controlled voltage-source converters," IEEE Transactions on Industrial Electronics, vol. 54, no. 6, pp. 3323–3334, 2007.

[24] T. Roinila, M. Vilkko, J. Sun, and S. Member, "Online Grid Impedance Measurement Using Discrete-Interval Binary Sequence Injection," IEEE Journal of Emerging and Selected Topics in Power Electronics, vol. 2, no. 4, pp. 985–993, 2014.

[25] D. Reigosa, F. Briz, C. B. Charro, P. Garcia, and J. M. Guerrero, "Active islanding detection using high-frequency signal injection," IEEE Transactions on Industry Applications, vol. 48, no. 5, pp. 1588–1597, 2012.

[26] A. Rygg and M. Molinas, "Apparent Impedance Analysis: A Small-Signal Method for Stability Analysis of Power Electronic-Based Systems," IEEE Journal of Emerging and Selected Topics in Power Electronics, vol. 5, no. 4, pp. 1474–1486, dec 2017. [Online]. Available: http://ieeexplore.ieee.org/document/7986961/

[27] M. Jaksic, Z. Shen, I. Cvetkovic, D. Boroyevich, R. Burgos, C. DImarino, and F. Chen, "Medium-Voltage Impedance Measurement Unit for Assessing the System Stability of Electric Ships," IEEE Transactions on Energy Conversion, vol. 32, no. 2, pp. 829–841, 2017.

[28] J. Schoukens, K. Godfrey, and M. Schoukens, "Nonparametric Data-Driven Modeling of Linear Systems: Estimating the Frequency Response and Impulse Response Function," IEEE Control Systems, vol. 38, no. 4, pp. 49–88, 2018. [Online]. Available: https://ieeexplore.ieee.org/document/8412623/

[29] P. Guillaume, J. Schoukens, R. Pintelon, and I. Kollái, "Crest-Factor Minimization Using Nonlinear Chebyshev Approximation Methods," IEEE Transactions on Instrumentation and Measurement, vol. 40, no. 6, pp. 982–989, 1991.

[30] J. Sun, "Small-signal methods for AC distributed power systems-A review," IEEE Transactions on Power Electronics, vol. 24, no. 11, pp. 2545–2554, 2009.

[31] G. Francis, R. Burgos, D. Boroyevich, F. Wang, and K. Karimi, "An algorithm and implementation system for measuring impedance in the D-Q domain," IEEE Energy Conversion Congress and Exposition: Energy Conversion Innovation for a Clean Energy Future, ECCE 2011, Proceedings, pp. 3221–3228, 2011.

[32] J. Huang, K. A. Corzine, and M. Belkhayat, "Small-Signal Impedance Measurement of Power-Electronics-Based AC Power Systems Using Line-to-Line Current Injection," IEEE Transactions on Power Electronics, vol. 24, no. 2, pp. 445–455, 2009.

[33] H. Alenius, R. Luhtala, and T. Roinila, "Amplitude Design of Perturbation Signal in Frequency-Domain Analysis of Grid-Connected Systems," in IFAC-PapersOnLine, 2020, pp. 1–6.

[34] J. Sun, "Impedance-based stability criterion for grid-connected inverters," IEEE Transactions on Power Electronics, vol. 26, no. 11, pp. 3075–3078, 2011.

[35] Y. Hu, S. Bu, B. Zhou, Y. Liu, and C.-W. Fei, "Impedance-Based Oscillatory Stability Analysis of High Power Electronics-Penetrated Power Systems—A Survey," IEEE Access, vol. 7, pp. 120 774–120 787, 2019.

[36] M. Belkhayat, "Stability criteria for AC power systems with regulated loads," Doctoral thesis, Purdue University, 1997.
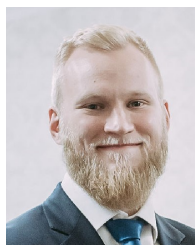
HENRIK ALENIUS (S'18) received his M.Sc. degree in electrical engineering from Tampere University of Technology, Tampere, Finland, in 2018. Since then, he has worked as a doctoral student with the Faculty of Information Technology and Communication Sciences at Tampere University. His research interests include impedance-based interactions in grid-connected systems, broadband methods in impedance measurements, and stability analysis of multi-parallel inverters.

RONI LUHTALA (S'17) received his M.Sc. in electrical engineering from the Tampere University of Technology, Tampere, Finland, in 2017. Since then, he has been working as a doctoral student in the Faculty of Engineering and Natural Sciences at Tampere University. His main research interests include real-time identification and adaptive control of grid-connected systems.
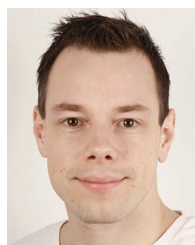
TOMI ROINILA (M'10) received the M.Sc. (Tech.) and Dr.Tech. degrees in automation and control engineering from Tampere University of Technology, in Finland, in 2006 and 2010, respectively. He is currently an assistant professor in the Faculty of Information Technology and Communications Sciences in Tampere University, in Finland. His main research interests include modeling and control of grid-connected power-electronics systems, and modeling of multiconverter systems.

• • •